Available online at www.sciencedirect.com
SCIENCE DIRECT®
ELSEVIER
Earth and Planetary Science Letters 214 (2003) 251–266
EPSL
www.elsevier.com/locate/epsl

Stalagmite growth and palaeo-climate: the numerical perspective

Georg Kaufmann *

Institut für Geophysik, Universität Göttingen, Herzberger Landstrasse 180, 37075 Göttingen, Germany

Received 28 February 2003; received in revised form 1 July 2003; accepted 1 July 2003

Abstract

The growth of stalagmites can be approximated by a simple mathematical model, which depends on growth rate and equilibrium radius. These two parameters are controlled by the climate. Temperature variations derived from ice and deep-sea core data, together with models for changes in precipitation and soil cover, are used to derive stalagmite stratigraphies, which reflect the palaeo-climate variations imposed. In general, stalagmite growth is strongly correlated to temperature and the amount of carbon dioxide available in the soil. Furthermore, precipitation is correlated to the stalagmite diameter. However, several assumptions need to be made: (i) A functional relationship between temperature on the one hand and precipitation and soil cover on the other needs to be established. (ii) The kinetics of calcite dissolution and precipitation needs to be assigned, either under soil and epikarst conditions open to the atmosphere or under fractured rock conditions closed from the atmosphere. These assumptions are difficult to access from field data, and therefore a stalagmite stratigraphy can be ambiguous and not easily converted back into an unknown palaeo-climate signal.

Keywords: stalagmite; speleothem; palaeo-climate; modelling

1. Introduction

The Earth's climate has undergone dramatic variations during the last 1 million years. Several cycles of roughly 100 000 yr duration have seen large ice sheets growing on continental areas during glacial periods, which then quickly collapsed, leaving the Earth in an interglacial stage as today. Simultaneously, the sea level has fluctuated by more than 100 m during the glacial cycles, and vegetation zones have moved hundreds of kilometres.

Unravelling the climate variations controlling the ice-age cycles is a primary goal in scientific research. Several archives recording climate information such as isotopic variations and changes in vegetation are used to study the palaeo-climate: ice cores and deep-sea cores dating back to more than 400 000 yr BP represent the marine record, while pollen and loess stratigraphies record the terrestrial variations. Speleothems, the calcite deposits common in cave environments [1], also contain valuable information about climate change,

* Tel.: +49-551-397462; Fax: +49-551-397459.
E-mail address: gkaufman@uni-geophys.gwdg.de (G. Kaufmann).

0012-821X/03/$ – see front matter © 2003 Elsevier B.V. All rights reserved.
doi:10.1016/S0012-821X(03)00369-8

both in their stratigraphy and the variation of stable isotopes. Frequently, stalagmites and flowstones are dated and their oxygen-isotope and carbon-isotope content is analysed to derive palaeo-climate information, e.g. from stalagmites in Oman [2,3], in Israel [4,5], in North America [6], in the European Alps [7–9], in Italy [10], and in Germany [11].

A number of studies [12–14] employ measured growth rates of speleothems (stalagmites and flowstones), and compare them to modelled growth rates based on mathematical models for the precipitation of calcite [15–18]. Baker et al. [12] have measured growth rates in the range of 0.01–0.05 mm yr^{-1} from three sites in southeast England and find a satisfactory agreement with modelled growth rates. However, the modelled growth rates, which are derived under the assumption of high drip rates, overestimate the measured growth rates by a factor of two to five. Baker et al. [13] have extended the measured growth rates to encompass sites in Belgium and France, and employed a more complicated model for growth including drip-rate dependence [19]. Measured and modelled growth rates agree well within the assumed uncertainty. More recently, Genty et al. [14] collected data from six cave sites throughout Europe, measuring drip-water chemistry and annual growth rates, and again were able to reconcile measured and modelled grow. Additionally, a good correlation between growth rates and both annual temperature and drip-water calcium concentration could be established, which indicates the significance of a palaeo-climate signal inscribed into the speleothems.

In this paper, we use a mathematical model to calculate stalagmite stratigraphies, based on palaeo-temperature variations derived from ice and deep-sea cores. We assess the potential of stalagmite stratigraphies to discriminate between different climate variations.

2. Stalagmite growth model

Speleothems in caves have a wide variety of shapes, ranging from simple straw stalactites and candlestick stalagmites, which are fed by punctiform drip sources, to more complicated forms such as canopies, shields, shelfstones, columns etc., which deposit from more complicated water sources (see [1] for a more comprehensive discussion). As we employ a simple mathematical model to determine stratigraphies [19–21], we need to focus on the simple form of a stalagmite, where water supersaturated with calcium is dripping from a point source. At this stage, we do not consider fall height of the drop or evaporation as significant. When a water drop hits the rock surface, a thin film of water spreads out radially, and CO_2 degasses from the solution. Calcite is precipitated in a thin layer around the impact area. At the centre, precipitation of calcite is greatest, and precipitation rates drop from the centre radially outwards. As the direction of crystal growth is directed perpendicularly to the surface of the stalagmite, growth continues upward and the stalagmite maintains its radius, as long as the prevailing equilibrium conditions do not change. Hence, changes in the shape of a stalagmite reflect changes in climate.

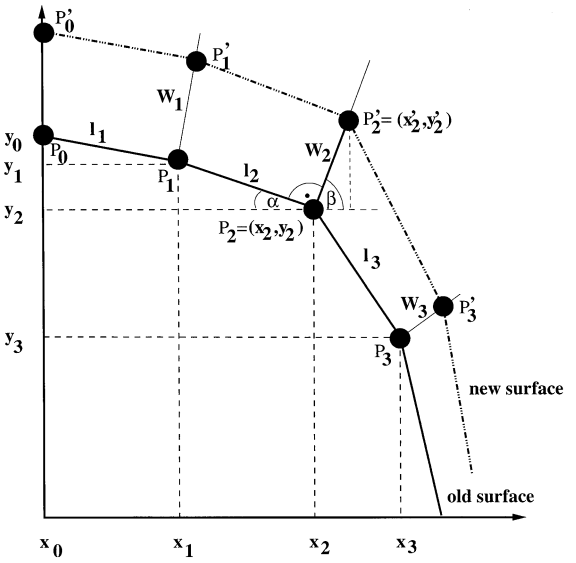

Fig. 1. Geometry of stalagmite surfaces.

2.1. Geometry

In Fig. 1, the old stalagmite surface is given by the polygon with points P_i, $i = 0, n$ from the centre

outwards. Each point P_i can be described in Cartesian coordinates (x_i, y_i), and the length segment between neighbouring points is described by the relation $l_i = \sqrt{(x_i - x_{i-1})^2 + (y_i - y_{i-1})^2}$, $i = 1, n$. The polygon length of the surface then is $\Sigma_i\, l_i$.

After a time step Δt, a new surface has been deposited, which is given by polygon points P'_i. This new surface is derived by assuming that each new point P'_i is located perpendicular to the old surface, and the distance from the old point P_i is calculated from the growth rate W_i:

$$W_i = W_0 \exp\left(-\sum_i l_i / R_0\right) \tag{1}$$

with R_0 the equilibrium radius of the stalagmite and W_0 the maximum growth rate at the centre of the stalagmite. Both R_0 and W_0 depend on climatic conditions and thus control the growth of a stalagmite, as will be explained in the next sections. However, we first deduce the iteration scheme used to calculate the new surface from an old one. The new coordinates are derived from the relation:

$$\begin{aligned} x'_i &= x_i + W_i \cos \beta_i \\ y'_i &= y_i + W_i \sin \beta_i \end{aligned} \tag{2}$$

where

$$\begin{aligned} \beta_i &= 90 - \alpha_i \\ \alpha_i &= \sin^{-1}\left(\frac{y_i - y_{i-1}}{l_i}\right) \end{aligned} \tag{3}$$

and W_i is derived from Eq. 1.

2.2. Growth rate and equilibrium radius

The growth rate of stalagmites can be derived either from numerical modelling or experiments on deposition rates of calcite. Deposition and precipitation rates of calcite within the ternary system H_2O–CO_2–$CaCO_3$ (water, carbon dioxide, calcite) have been studied theoretically [17,18]. The theoretically derived rates have been verified experimentally [22,23]. It has been shown that the kinetics of the calcite deposition and precipitation is controlled by three processes: (i) The chemical reactions at the crystal surface described by the PWP-equation [24]; (ii) the slow conversion of HCO_3^- and H^+ into CO_2 and H_2O in the solution [25], which becomes important for small water film thicknesses, and (iii) mass transport of the dissolved species by diffusion.

2.2.1. Growth rates

The maximum deposition rate F (in mol m^{-2} s^{-1}) can be approximated by the linear relation [13]:

$$F = \alpha(c - c_{\mathrm{app}}) \tag{4}$$

with α a rate constant (in m s^{-1}) as given in [13,19], and c (in mol m^{-3}) the actual calcium concentration in the dripping water, which depends on the soil cover and the type of pathway through the rock. c_{app} (in mol m^{-3}) is the apparent calcium concentration at equilibrium [23], which is above the calcium concentration at equilibrium, c_{eq} (in mol m^{-3}), a result of the inhibiting effect of precipitation studied by [26] and [21]. While the rate constant α depends on temperature T (in °C) and the thickness of the water film δ (in m), the apparent calcium concentration c_{app} is a function of temperature and CO_2 pressure p_{cave} (in atm) in the cave:

$$\alpha = \alpha(T,\ \delta)$$

$$c_{\mathrm{app}} = c_{\mathrm{app}}(T,\ p_{\mathrm{cave}})$$

We fix the film thickness to $\delta = 0.01$ cm, which is in agreement with measurements from [21] and [13]. For the CO_2 pressure in the cave, we assume a constant value of $p_{\mathrm{cave}} = 400$ ppm, which is in accordance with measurements reported in [13]. As the latter assumption affects the growth rate by a factor of two, we note that the growth rates reported here are maximum growth rates; in caves with higher CO_2 concentrations, stalagmite growth will be slower [12].

The maximum deposition rate Eq. 4 is only achieved for high drip rates, which we express as drip interval Δd (in s). If the drip rate is low, and hence the drip interval Δd is large, the deposition rate drops to lower values. Converting the deposition rates F into growth rates W_0 (in m yr^{-1}), the drip-rate-dependent growth is expressed as [19]:

$$W_0 = 1.174 \times 10^3 (c - c_{\mathrm{app}}) \frac{\delta}{\Delta d}\left[1 - \exp\left(-\frac{\alpha}{\delta}\Delta d\right)\right] \tag{5}$$

For low drip rates, a minimum growth rate can be derived:

$$W_0^{\min} = 1.174\times10^3(c-c_{\mathrm{app}})\,\frac{\delta}{\Delta d},\ \Delta d \gg \frac{\delta}{\alpha} \tag{6}$$

while for high drip rates, the growth rate reaches a maximum:

$$W_0^{\max} = 1.174\times10^3(c-c_{\mathrm{app}})\,\alpha,\ \Delta d \ll \frac{\delta}{\alpha} \tag{7}$$

2.2.2. Equilibrium radius

The equilibrium radius of a stalagmite can be derived from the following consideration: Under equilibrium conditions, water flowing across the stalagmite surface loses all excess calcium and the stalagmite grows vertically upwards, while keeping its shape [27]. Then, the amount of calcium deposited onto the surface within a given time interval is equal to the supersaturation of the drop, $(c-c_{\mathrm{app}})$. From this consideration, an equilibrium radius R_0 (in m) can be derived [21,19]:

$$R_0 = \sqrt{\frac{V}{\pi\delta\left[1-\exp\left(-\frac{\alpha}{\delta}\Delta d\right)\right]}} \tag{8}$$

with V the drop volume (in m^3) and Δd the time interval between two drops (in s). Typical drop volumes are in the order of $V \simeq 0.1$ cm^3 [28], while drip intervals can vary significantly, $\Delta d \in [1, 10^6]$ s. Here, small values correspond to high-flow regimes, large values to low-flow regimes. From Eq. 8, two asymptotic values can be deduced, the low-flow diameter:

$$R_0^{\min} = \sqrt{\frac{V}{\pi\delta}},\ \Delta d \gg \frac{\delta}{\alpha} \tag{9}$$

and the high-flow diameter:

$$R_0^{\max} = \sqrt{\frac{V}{\pi\alpha\Delta d}},\ \Delta d \ll \frac{\delta}{\alpha} \tag{10}$$

For low flow rates, R_0 depends on drop volume and film thickness, while for high flow rates, R_0 depends on precipitation kinetics and drip rates.

Both the growth rate W_0 and the equilibrium radius R_0 are functions of several parameters, which depend on climatic conditions. Using the fundamental parameters temperature T, CO_2 pressure p, and drip interval Δd, the dependences read:

$$W_0 = W_0(T,\ p,\ \Delta d)$$

$$R_0 = R_0(T,\ \Delta d)$$

Both W_0 and R_0 depend on temperature and drip interval, but while the growth rate W_0 also depends on the CO_2 pressure p, and therefore the calcium excess concentration in the drop, the equilibrium radius R_0 is independent of it. The parameter dependence of growth rate and equilibrium radius is shown in Fig. 2. For the temperature and drip-interval ranges considered, the growth rate is always below 0.25 mm yr^{-1}. For large drip intervals ($\Delta d > 1000$ s) corresponding to low precipitation rates, the growth rate is almost independent of temperature and increases with smaller drip intervals. If the climate is more humid ($\Delta d < 1000$ s), temperature also controls the growth rate. Comparing the growth rates for two different CO_2 concentrations, it is obvious that the vegetation dominates the growth-rate signal. Equilibrium diameters mainly depend on the drip interval. For drip intervals larger than $\Delta d \simeq 1000$ s, a minimum equilibrium diameter is established ($R_0^{\min} \simeq 4$ cm), as predicted by Curl [28]. Diameters above the 20 cm range require shorter drip intervals around $\Delta d \simeq 10$–100 s. Note that the generation of massive cone-shaped stalagmites with

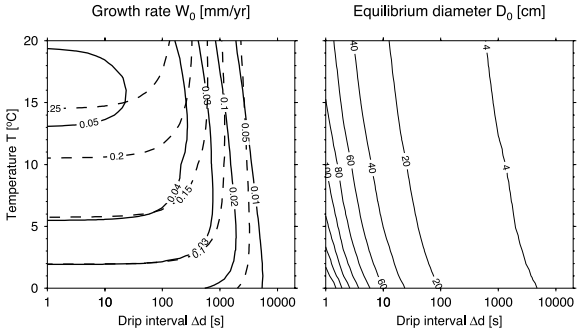

Fig. 2. Growth rate W_0 and equilibrium diameter D_0 as a function of temperature and drip interval. The growth rate is shown for two CO_2 concentrations: $p = 0.02$ atm (solid lines) and $p = 0.05$ atm (dashed lines). Values are derived for the closed system.

diameters in the meter range need both short drip intervals and low temperatures.

3. Calcium and CO_2 concentrations

Stalagmite growth is only possible if the water dripping into a cave is supersaturated with calcium. Therefore the water needs high CO_2 concentrations from the vegetation cover. If water seeps underground through bare rock, the CO_2 concentration is too low and, instead of precipitation, corrosion may occur in the cave.

If the water is supersaturated with calcium, on entering the cave CO_2 is degassed from the drop and the excess calcium Δc is deposited as calcite (or aragonite) in the cave. The amount of calcite deposited depends on the calcium equilibrium concentration c_{eq} of the drop in the cave atmosphere.

Generally, the calcium equilibrium concentration depends on the temperature T and the initial carbon-dioxide partial pressure $p = p_i$ of the solution. An analytical relation derived for a simplified charge balance reads [21]:

$$c_{eq}^3 = \frac{K_1 K_C K_H}{4 K_2 \gamma_{Ca^{2+}} \gamma_{HCO_3^{2+}}^2} p \qquad (11)$$

with K_1, K_2, K_C, and K_H reaction equilibrium parameters and $\gamma_{Ca^{2+}}$ and $\gamma_{HCO_3^{2+}}$ activity coefficients for calcium and bicarbonate (Table 1). Eq. 11 is valid for the open system, in which the solution is in contact with the atmosphere. Under closed-system conditions, however, the carbon-dioxide concentration in the solution decreases with time, as dissolution proceeds. In this case, p in Eq. 11 needs to be replaced by:

$$p = p_i - \frac{c_{eq}}{K_H\left(1 + \frac{1}{K_0}\right)} \qquad (12)$$

with p_i the initial carbon-dioxide concentration and K_0 a reaction equilibrium parameter (Table 1). Inserting Eq. 12 into Eq. 11 yields a cubic equation for the calcium equilibrium concentration, which needs to be solved to derive the calcium equilibrium concentration corresponding to an initial carbon-dioxide partial pressure. While the carbon-dioxide partial-pressure dependence is explicitly seen in Eq. 11, the temperature dependence is given through the temperature-dependent reaction equilibrium coefficients (see Table 1).

The non-linear dependence of the calcium equilibrium concentration on carbon-dioxide partial pressure can be seen in Fig. 3. In a typical cave atmosphere ($T_{cave} = 10°C$, $p_{cave} = 400$ ppm), the calcium equilibrium concentration is around $c_{eq} \simeq 0.6$ mol m^{-3}, as indicated by the grey-shaded area. Stalagmite growth in this cave atmosphere

Table 1
Kinetic parameters

Parameter	Description	Unit	Value
T_c	Temperature	[°C]	0–20
T	Temperature	[K]	$273.16+T_c$
I	Ion activity	[–]	$3c$
A[a]	Debye–Hückel coefficient	[–]	$0.4883+8.074\times10^{-4}T_c$
B[a]	Debye–Hückel coefficient	[–]	$0.3241+1.600\times10^{-4}T_c$
log γ_{CA}[b]	Activity coefficient	[–]	$-4A\sqrt{I}/(1+5.0\times10^{-8}\ B\sqrt{I})$
log γ_{HCO_3}[b]	Activity coefficient	[–]	$-1A\sqrt{I}/(1+5.4\times10^{8-}\ B\sqrt{I})$
log K_0	Mass balance coefficient	[–]	K_5/K_1
log K_1[c]	Mass balance coefficient	[mol l^{-1}]	$-356.3094-0.06091964T+21\,834.37/T+126.8339$ log $T-1\,684\,915/T^2$
log K_2[c]	Mass balance coefficient	[mol l^{-}1]	$-107.8871-0.03252849T+5151.79/T+38.92561$ log $T-563\,713.9/T^2$
log K_5[c]	Mass balance coefficient	[mol l^{-1}]	1.707×10^{-4}
log K_C[c]	Mass balance coefficient	[mol^2 l^{-}2]	$-171.9065-0.077993T+2839.319/T+71.595$ log T
log K_H[c]	Mass balance coefficient	[mol l^{-1} atm^{-1}]	$108.3865+0.01985076T-6919.53/T-40.45154$ log $T+669\,365/T^2$

[a] From [43].
[b] From [44].
[c] From [42].

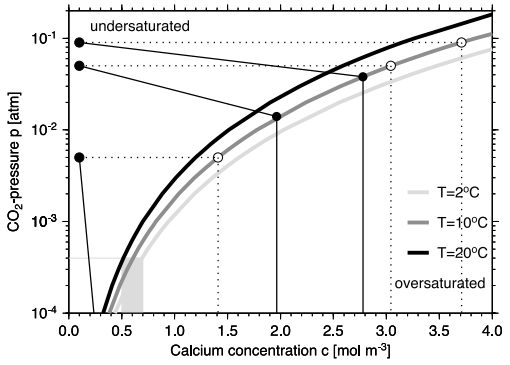

Fig. 3. Calcium equilibrium concentration as a function of partial carbon-dioxide pressure for three temperatures ($T=2$, 10, 20°C). In the open system, dissolution proceeds along horizontal (dashed) lines, while in the closed system dissolution proceeds along sloping (solid) lines. The grey area indicates calcium concentrations in equilibrium with a typical cave atmosphere.

will only initiate when the actual calcium concentration c is above the apparent calcium equilibrium $c_{app} \simeq 1.2 c_{eq}$ ($c > 0.7$ mol m^{-3}). An excess concentration $\Delta c = c - c_{app}$ therefore needs a solution with higher carbon-dioxide concentrations. Given that the atmospheric CO_2 concentration is around $p_{atm} \simeq 340$ ppm, we need additional sources of CO_2 for speleothem deposition. These usually result from organic activity in the soil, where CO_2 concentrations can be as high as 100 000 ppm. As a first approximation, we can deduce a dependence of CO_2 concentration on temperature, as soil generation and organic activity depend on the climatic conditions.

However, a further complication arises from the complex pathway the water can take on its way down to a cave. Precipitation seeping down into the karst passes through soil, the epikarst, and the fractured carbonate rock, and finally reaches an air-filled cave, where calcite deposition might occur. Several situations can arise: (i) Water takes up CO_2 in the soil, and dissolves limestone mainly in the soil and in the epikarst. In this case dissolution occurs under open-system conditions, as the solution is still in contact with the atmosphere. Assuming CO_2 concentrations around $p = 0.05$–0.1 atm, the water can dissolve up to 3–3.7 mol m^{-3} calcium (dashed lines in Fig. 3), resulting in a large excess concentration around $\Delta c \simeq 2.3$–3 mol m^{-3}. (ii) Water takes up CO_2 in the soil, but dissolves limestone mainly in the narrow water-filled fissures below the epikarst zone. In this case, dissolution occurs under closed-system conditions, and the CO_2 concentration in the solution decreases according to Eq. 12. As a consequence, calcium concentrations are much lower, reaching only 2–2.8 mol m^{-3} (solid lines in Fig. 3), and consequently the calcium excess concentrations are only around $\Delta c \simeq 1.3$–2 mol m^{-3}. Thus, the calcium excess concentration Δc also depends on the pathway of the seepage water, which is very difficult to assess and which may vary significantly even over a small area.

4. Results for simple models

Based upon the theory derived in the previous sections, we discuss stalagmite growth for a simple climate model (Table 2), which depicts the last interglacial from 10 000 yr to the present. We compare several growth models, in which only one of the controlling parameters temperature, CO_2 concentration, and drip interval is varied. For each of these scenarios, the two extreme cases for seepage water, dissolving under open- and closed-system conditions, are discussed.

The first model establishes a reference case, and assumes constant parameters throughout the interglacial. Results are shown in Fig. 4. Typical values chosen are $T = 10$°C, $p = 0.03$ atm, and $\Delta d = 100$ s (Fig. 4a). For these parameters, constant growth rates of 0.3 mm yr^{-1} under open-system conditions and 0.1 mm yr^{-1} under closed-system conditions result, and the equilibrium diameter is around 10 cm (Fig. 4b). The resulting stalagmites are evenly growing candlestick stalagmites, which only differ in their height according to the prevailing flow conditions of the seepage water.

For the second model, we assume a temperature increase over the entire period from 0 to 10°C, while all other parameters are kept fixed (Fig. 5a). As temperature controls both the growth rate and the equilibrium radius, changes can be seen in Fig. 5b: Growth rates increase about a factor of three for both open- and closed-

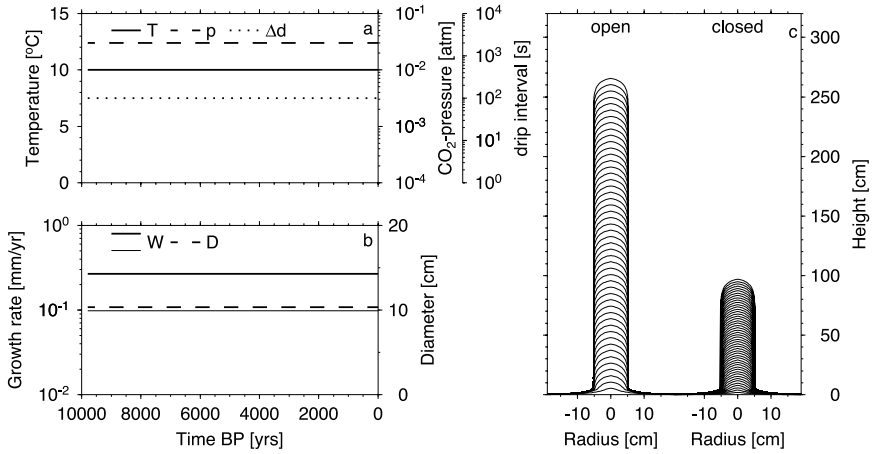

Fig. 4. Stalagmite growth during the last 10 000 yr under open and closed flow conditions: Constant climatic conditions. (a) Temperature T, CO_2 concentration p, and drip interval Δd. (b) Growth rates W_0 for open (thick line) and closed (thin line) system conditions, and equilibrium diameter D_0. (c) Stalagmite shape for open- and closed-system conditions. Shapes are redrawn every 200 yr.

system cases. Simultaneously, the equilibrium diameter decreases from around 16 to 10 cm, independent of the percolation pathway. In both cases, a tapered stalagmite develops (Fig. 5c), which again differs only in the height reached.

In the third model, the CO_2 concentration increases from 0.003 to 0.03 atm during the interglacial, with the remaining parameters fixed (Fig. 6a). As the change in carbon dioxide only affects the calcium excess concentration, only growth rates are affected, while the equilibrium diameter remains constant (Fig. 6b). However, the one order of magnitude increase in CO_2 concentration results in a change of the growth rate of about one order of magnitude. Consequently, we again obtain stalagmites with constant diameter as in the first model, but now they are less tall, as growth was slow during the early phase.

The fourth model simulates a one order of magnitude change in drip intervals from one drop per 1000 s to one drop per 100 s, with all other parameters kept fixed (Fig. 7a). Growth rates in this case increase by a factor of two, while the equilibrium diameter increases from around 4 to 10 cm (Fig. 7b). The resulting shapes resemble club-like stalagmites (Fig. 7c), which again differ

Table 2
Model parameters for stalagmite growth

Climate			
T	Temperature	[°C]	0–20
p	CO_2 pressure in drop	[atm]	3×10^{-4}–10^{-1}
Δd	Drip interval	[s]	1–10^6
Kinetics			
α	Kinetic rate constant	[m s^{-1}]	$(4–30)\times10^{-8}$
c_{in}	Calcium concentration in drop	[mol m^{-3}]	0–4
c_{eq}	Calcium equilibrium concentration	[mol m^{-3}]	0–1
c_{app}	Apparent calcium equilibrium concentration	[mol m^{-3}]	$1.12\times c_{eq}$
Fixed			
δ	Film thickness	[m]	10^{-4}
V	Drop volume	[m^3]	10^{-7}
p_{cave}	CO_2 pressure in cave atmosphere	[atm]	4×10^{-4}
m_r	Molecular weight of $CaCO_3$	[kg mol^{-1}]	0.10009
ρ_c	Density of $CaCO_3$	[kg m^{-3}]	2689

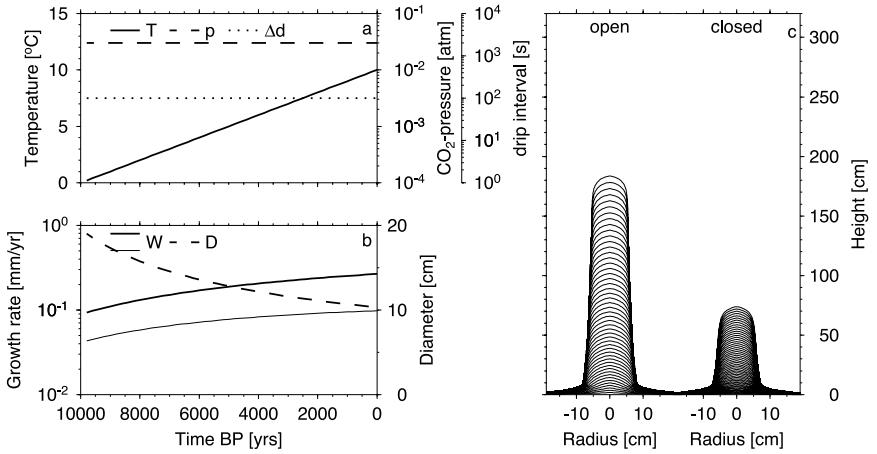

Fig. 5. As Fig. 4, but for temperature increase.

in their final height, depending on the pathway of seepage water.

The changes in stratigraphy and form found in these simple models agree with earlier inferences from Dreybrodt [19], who noted that for climatic variations with a period longer than that required to obtain equilibrium growth (200–2000 yr), the stratigraphy is recording the climatic change. Keeping in mind the above results, we proceed to more realistic climate-change scenarios.

5. Climate control

The complex interdependence of stalagmite growth and palaeo-climate needs to be parameterised for a more realistic numerical model, and therefore several assumptions and simplifications need to be made.

5.1. Temperature

We start discussing these dependences by introducing the atmospheric temperature T as a master variable. We separate T into a spatial part T_1 depending on geographical location (latitude θ, longitude ϕ) and altitude (h), and a time-dependent part T_2 (time t) simulating the temperature variations during the ice-age cycles:

$$T = T_1(\theta,\ \phi,\ h) + T_2(t) \tag{13}$$

While T_1 can be chosen as the average annual

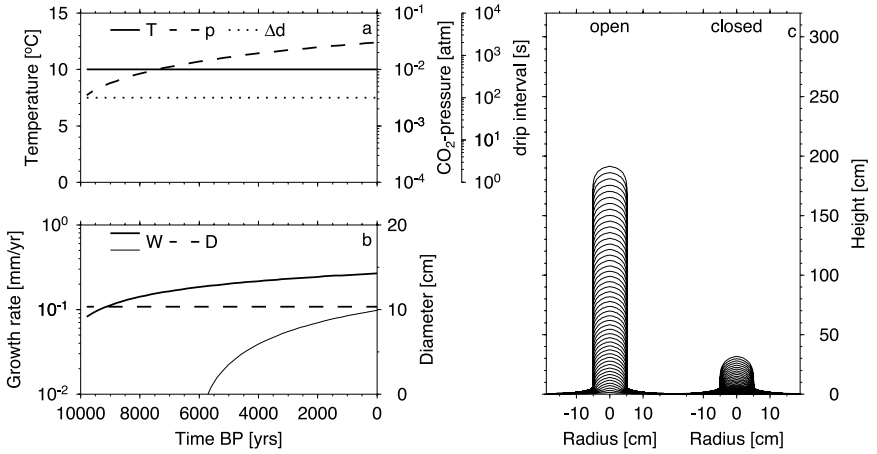

Fig. 6. As Fig. 4, but for CO_2 increase.

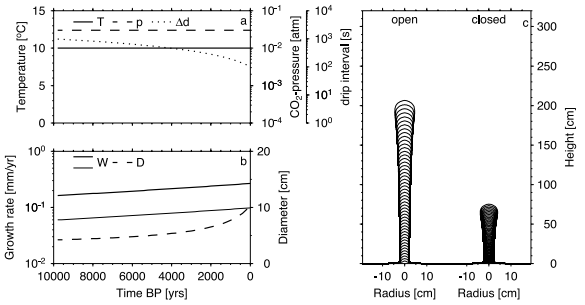

Fig. 7. As Fig. 4, but for drip-interval decrease.

temperature at a given cave location, T_2 is assumed to be known from palaeo-climate data, e.g. ice cores, when the numerical forward model of stalagmite growth is considered. Most palaeo-temperature records are recovered from either ice cores such as the Greenland GRIP ice core [29,30], or the Antarctic Vostok ice core [31], or from marine sediment cores such as the V19-30 SPECMAP core [32,33]. Note that these palaeo-temperature records do not necessarily reflect the temperature variations at a specific continental cave site, where a stalagmite sample has been taken.

As a present-day reference temperature, we choose $T_1 = 10°C$, which is a characteristic value for middle European sites [34]. For the time-dependent change in temperature T_2, we adopt several scenarios: A first simple parameterisation represents a temperature difference of 10°C between glacials and interglacials for four ice-age cycles simulated with a sawtooth function (light grey area in Fig. 8). The 0°C for glacials result in no stalagmite growth, while the 10°C for interglacials favour stalagmite growth.

Two temperature functions are taken from ice core data: Data from the Vostok ice core in East Antarctica (78°S, 106°E, 3488 m asl, 3623 m core length) include profiles of the deuterium variation of the ice δD_{ice}. The deuterium is linearly related to the temperature above the inversion level, and from this temperature the variation in surface temperature has been derived [31]. Combining the surface temperature log with a timescale derived from the core depth and ice-flow as well as mass-balance modelling [35], the palaeo-temperature variation shown in Fig. 8 has been derived. The record extends over four glacial cycles, is characterised by a clear 100 000 yr signal, and some smaller variations during each glacial cycle. The temperature range between glacials and interglacials is around 12°C, and the average temperature and its variance is $\overline{T}_2 = 5.23 \pm 2.77°C$.

For the GRIP ice core in Greenland (72.57°N, 37.62°E, 3246 m asl, 3028 m core length), temperatures are derived from the oxygen-isotope profile $\delta^{18}O_{ice}$, using a non-linear relation between the oxygen isotope record and palaeo-temperatures [36,37]. The timescale for the GRIP ice core is derived from counting annual layers for times younger than 14 000 yr BP, and extended by ice-

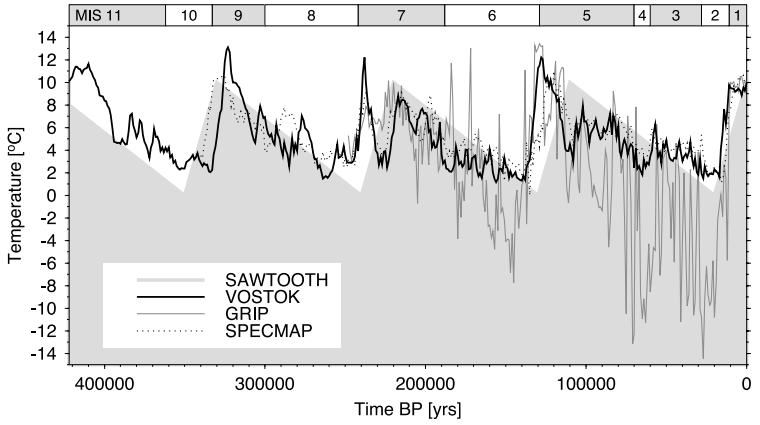

Fig. 8. Temperature functions for stalagmite growth. Temperatures are based on stable isotope records of either ice cores (GRIP and VOSTOK) or marine cores (SPECMAP). The grey-shaded area depicts a simple sawtooth-temperature function for four glacial cycles. Numbers and blocks above the figure indicate the marine isotope stages (MIS).

flow and heat-transport modelling before that time. The record extends over two glacial cycles, with a large glacial–interglacial temperature contrast of around 20°C. The variation of temperatures during a glacial cycle is also very pronounced for this core, with is attributed to rapid changes in the ocean/atmosphere circulation in the North Atlantic [30]. The average temperature and its variance is $\overline{T}_2 = 2.31 \pm 6.10$°C. This average is significantly lower than for the Vostok ice core, but the large variance reflects the much larger fluctuations during a cycle.

For comparison, we have used the SPECMAP oxygen-isotope stack [38]. This dataset is recovered from marine core V19-30 (3°S, 83°W, −3091 m) and the $\delta^{18}O_{seawater}$ reflects changes in global ice volume, and covers three glacial cycles. For our purposes, we have rescaled this record into a temperature variation, with 11°C during interglacials, and 0°C during glacials. The average temperature and its variance is $\overline{T}_2 = 5.48 \pm 2.23$°C. As in the Vostok temperature data, a clear 100 000 yr signal is visible, but variations during each glacial cycle are much smaller.

5.2. CO_2 concentration and precipitation

Two more climate variables need to be known for the stalagmite-growth reconstruction, palaeo-precipitation and changes in the carbon-dioxide concentration (CO_2 variation) in the soil. Both quantities are difficult to reconstruct from palaeo-records. We adopt a simple approximation: For CO_2 variations, we argue that during cold glacial phases no soil has been present on the karst surface, hence water seeping down into the rock was in equilibrium with the low atmospheric CO_2 concentration, defined as $p_{min} \simeq 340$ ppm. During warmer interglacials, a soil cover was present, and due to organic activity the CO_2 concentration was considerably higher, up to levels of $p_{max} \simeq 40\,000$ ppm at 20°C. For the palaeo-precipitation, we assume high precipitation rates during interglacials, as the weather was more dynamic due to higher temperatures. Hence the drip interval in the cave has been at a minimum, $\Delta d_{max} \simeq 10$ s. During the peak glacial phases, precipitation was retained at the surface as snow and ice, hence drip intervals have been very large, $d_{min} \to \infty$. We assume a linear relation of both p and Δd with palaeo-temperature T:

$$p(T) = p_{min} + \frac{p_{max} - p_{min}}{T_{max} - T_{min}} (T - T_{min}) \quad (14)$$

$$\Delta d(T) = \Delta d_{min} + \frac{\Delta d_{max} - \Delta d_{min}}{T_{max} - T_{min}} (T - T_{min}) \quad (15)$$

Here, T_{min} and T_{max} are the temperature extremes of the ice-age cycles. We also define a CO_2 concentration in the cave atmosphere, $p_{cave} = 400$ ppm, which is assumed to be constant. The dependences of the CO_2 variation and the drip interval on temperature are plotted in Fig. 9a,b. For temperatures below 0°C, p and Δd remain at their glacial values p_{min} and Δd_{min}, representing the glacial stage with bare rock surface and almost no water seeping down into the karst. For larger temperatures, both p and Δd increase towards their interglacial values p_{max} and Δd_{max}, which they reach at a temperature of 20°C. The CO_2 variation can be compared to a relation derived by Drake and Wigley [39]. Here, several karst springs in North America with water almost saturated with respect to calcite were studied, and a linear relation between CO_2 and temperature could be established. As shown in Fig. 9a, our model closely follows the model of [39] for temperatures above 5°C; below that, our CO_2 variation is considerably lower. Consequently, the model of [39] would enhance stalagmite grow at low temperatures.

Variations of the calcium excess concentration Δc are shown in Fig. 9c. The dependence on palaeo-climate in this case is more complicated, as both temperature and CO_2 concentration control the calcium excess (see Eqs. 11 and 12). Additionally, flow through either the open or the closed system is important. In the closed system, a calcium excess is only present above a temperature of 6°C, and from this threshold the calcium excess increases to 0.7 mol/m^3. If flow occurs under open-system conditions, precipitation is possible above 0°C in this model, and Δc increases to almost 2 mol/m^3.

This large difference in calcium excess concentration translates directly into differences in

growth rates, as can be seen in Fig. 10a. For warmer climates, growth rates for droplets percolating through the open system are twice as large as for the closed system. For the model chosen, maximum growth rates for both systems are around 0.6 and 0.3 mm yr^{-1}, respectively. The equilibrium diameter is shown in Fig. 10b. In contrast to the simple models discussed before, values now increase as temperature increases. This increase is caused by be strong dependence of the drip interval on temperature.

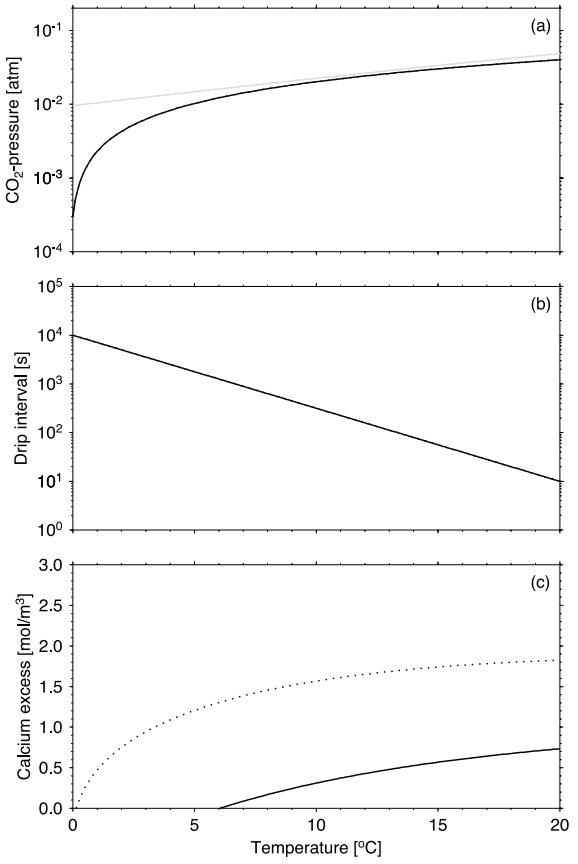

Fig. 9. (a) CO_2 pressure p, (b) drip interval Δd, and (c) calcium excess concentration Δc as a function of temperature. In panel a, the grey line indicates the soil-CO_2 pressure derived by Drake and Wigley [39]. In panel c, the dashed line is for the open-, the solid line for the closed-system case.

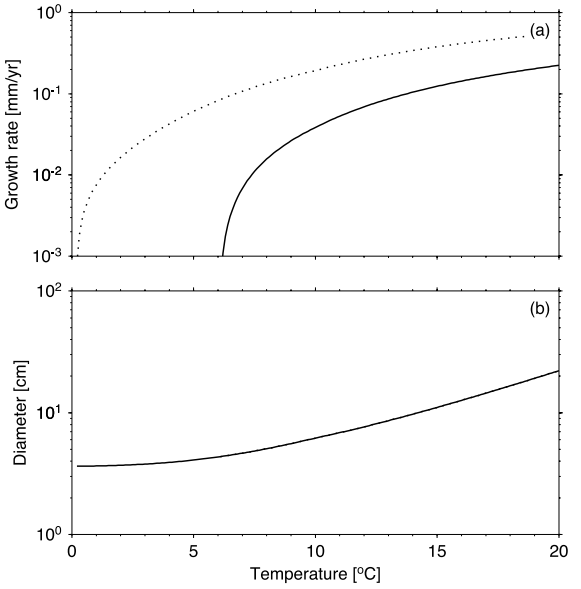

Fig. 10. Growth rate (a) and diameter (b) as a function of temperature. Dashed line is for the open-, solid line for the closed-system case.

6. Results for climate-driven models

6.1. Variations in palaeo-temperature

Now we have collected information about average present-day temperatures in Middle Europe, $T_1(\theta, \phi, h)$, various palaeo-temperature variations, $T_2(t)$, and we have established simple approximations to couple variations in precipitation and CO_2 change to the temperature. Using the four palaeo-temperature scenarios shown in Fig. 8, we start comparing the stratigraphies of stalagmites grown under these different palaeo-climate scenarios (Fig. 11), which are derived under closed-system conditions.

For the simple sawtooth-temperature function, the resulting SAWTOOTH-stalagmite reflects the four cycles of the simplified palaeo-temperature variation clearly. Maximum growth occurs during the interglacials, while hiatuses occur during peak glacial periods. As the driving temperature variation is the same for all four ice-age cycles, the stratigraphy is simply repeated for each cycle. During interglacials there is an increase in stalagmite diameter that corresponds to the intervals of

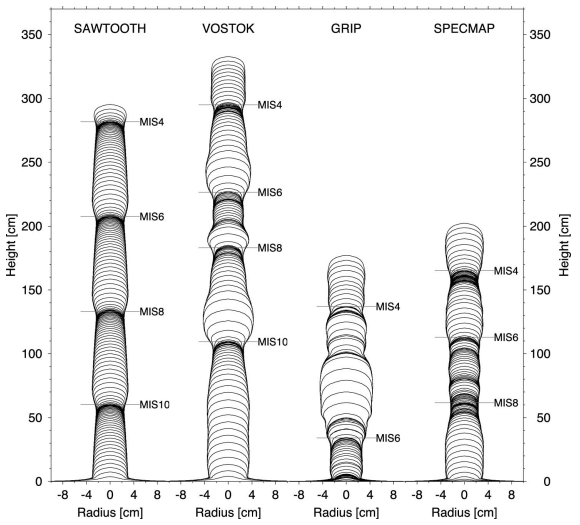

Fig. 11. Stratigraphies of stalagmites for different palaeo-temperature variations, as depicted in Fig. 8. Surfaces are redrawn every 1000 yr. The horizontal lines mark the beginning of glacial phases in the marine isotope record (MIS).

faster growth, while minima are found during peak glacial periods. Stalagmite growth is around 70 cm per glacial cycle, and the entire stalagmite is almost 3 m tall.

The Vostok temperature record covers the same four glacial cycles as the simple sawtooth function. However, due to the temperature variations in between each glacial cycle, the stratigraphy of the VOSTOK-stalagmite is much more complicated: We can still identify the four hiatuses corresponding to the peak glacial periods, but growth between the hiatuses is very different for each cycle, reflecting the temperature fluctuations recorded in the Vostok ice core. The cycle MIS 11–10 is characterised by rather smoothly falling temperature, hence the shape of the VOSTOK-stalagmite for this period is smooth (bottom cycle). The interglacial MIS 9 was very warm, which is reflected in the thick fast-growing section (second cycle). Similarly, the interglacial MIS 7 also was warm, and a large diameter again appears in the stratigraphy (third cycle). However, as temperature during MIS 7–6 was generally lower than during MIS 11–10, the stratigraphic section of the third cycle is short. The last cycle also had low temperatures, and the recent growth phase on top is very homogeneous, a result of the stable temperatures during MIS 1. The total length of the VOSTOK-stalagmite is around 3.3 m.

The GRIP temperature record only covers two glacial cycles, starting at MIS 7. As a consequence, the GRIP-stalagmite is much shorter, only around 1.8 m. More important, however, are the large temperature variations during the glacial cycles in the GRIP record. These large variations result in a complicated stratigraphy of the GRIP-stalagmite, and the hiatuses related to the peak glacial phases MIS 6 and MIS 4 are not easily identified. The two high-temperature peaks during MIS 6 boost growth during this period, but in between growth has stopped several times. During the last glacial cycle, temperatures according to the GRIP ice core have been very low, and growth was stopped for a long time between MIS 5 and MIS 2. Relative stable temperatures during the last interglacial MIS 1 produced a stable stratigraphy, similar to the last part of the VOSTOK-stalagmite.

The SPECMAP-stalagmite resulting from the temperature function derived from the SPECMAP record is around 2 m tall, just taller than the GRIP-stalagmite, despite the additional glacial cycle. While the peak glacial periods produce clear hiatuses in this stratigraphy, growth during the interglacials was low, because peak temperatures were never above 11°C. This is also reflected in the smaller variations in diameter, when compared to the GRIP-stalagmite.

Apart from the stratigraphy several other parameters can be studied in detail. Firstly, growth rates as a function of time are shown in Fig. 12a. For the SAWTOOTH-stalagmite, growth rates follow an asymmetrical shape, with steep increases at the beginning of an interglacial, and slower decreases during the build-up of the next glacial phase. The maximum growth rate is around 40 μm yr^{-1}, a reasonable value for stalagmites. Growth stopped during the glacial intervals, marking three clear and distinct hiatuses. For the VOSTOK-stalagmite, we observe larger growth rates, with maxima around 90 μm yr^{-1}. Growth begins at the beginning of MIS 9, 7, 5, and 1 with a sharp rise in growth rates, but growth then only lasts for about 20 000 yr. During

MIS 7, two more growth periods are present due to the higher temperatures, resulting in additional hiatuses. For the GRIP-stalagmite, growth behaviour is even more flashy: While growth also starts at the beginning of the interglacials, the large temperature fluctuations interrupt the growth period and therefore additional hiatuses are generated. The large temperature variations during MIS 6 result in peak growth rates above 100 μm yr^{-1}. The SPECMAP-stalagmite grows more uniformly, but with less than 60 μm yr^{-1} peak growth rates are lower. Also the individual growth phases are mostly shorter than 15 000 yr. When we compare the maximum growth rates to field data, our calculated values ranging between 50 and 100 μm yr^{-1} are more typical for warm-temperature climates such as Oman, where Neff et al. [3] show maximum growth rates of around 600 μm yr^{-1}. Observed growth in cold-temperature climates such as the European Alps is much lower, with values between 15 and 35 μm yr^{-1} as reported by Wurth et al. [8].

Secondly, the equilibrium diameter is very sensitive to the temperature function driving the stalagmite growth, as can be seen in Fig. 12b. The regular palaeo-temperature variations for the sawtooth-history are reflected in the regular pattern of equilibrium diameters for the SAWTOOTH-stalagmite. During interglacials MIS 9, MIS 7, and MIS 5, the diameters are around 5 cm, with little variation during each interglacial. In contrast, the VOSTOK-stalagmite exhibits variations in diameter between 4 and 9 cm during peak interglacials. Clearly visible are the strong growth phases of MIS 9, MIS 7, and MIS 5 triggered by the temperature peaking around 12°C. Similarly, the GRIP-stalagmite also shows variations in diameter between 4 and 9 cm, and due to the very strong temperature variations recorded in this ice core, the recorded signal is very often interrupted, as already discussed for the stratigraphy. Finally, the SPECMAP-stalagmite shows again a smoother variation in diameter, clearly related to the smoother palaeo-temperature signal present in this deep-sea sediment core.

We conclude that the key parameters of stalagmite growth, the growth rate and the equilibrium diameter, are very sensitive to different palaeo-climate scenarios, and thus a stalagmite from a particular region is a unique record of climate variability in that region. However, more local climate parameters such as variations in soil activity and precipitation events will obscure the stalagmite record on a regional scale, as we discuss next.

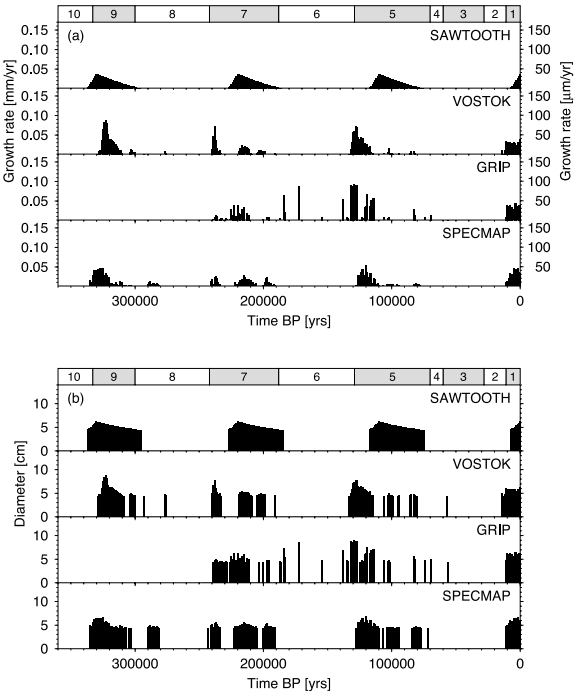

Fig. 12. (a) Growth rate W_0, and (b) equilibrium diameter D_0 for stalagmites shown in Fig. 11. Numbers and blocks above the figure indicate the marine isotope stages (MIS).

6.2. Variations in palaeo-precipitation

We discuss the evolution of growth for the GRIP-stalagmite under different precipitation regimes. Hence, we assume a common regional temperature variation for the cave location discussed, but allow for local changes in precipitation due to rain shadowing or channelling of water on the surface. We vary the minimum drip interval corresponding to precipitation during interglacials. The standard regime used before was one drop every 10 s ($\Delta d_{max} = 10$ s). We compare this model with a wet regime ($\Delta d_{max} = 1$ s) and a dry regime ($\Delta d_{max} = 100$ s). The corresponding stratigraphies

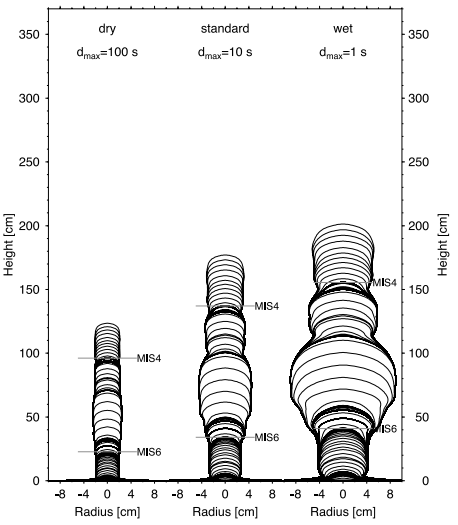

Fig. 13. Stratigraphies of stalagmites with different drip intervals. The palaeo-temperature variation is taken from the GRIP ice core (Fig. 8), and drip intervals are given in the legend. Surfaces are redrawn every 1000 yr.

are shown in Fig. 13. As the drip interval influences both the growth rate and the equilibrium diameter, the three different stalagmites have reached different heights and their diameters vary.

Compared to the standard regime (middle) with a total height of around 1.8 m, the dry regime (left) results in a stunted stalagmite only 1.2 m tall. This is a result of the reduced growth rates, which are only 80 μm yr^{-1} at peak growth compared to 100 μm yr^{-1} for the standard regime. Also the reduction in drip rate results in a less irregular shape of the stalagmite, as variations in diameter are very limited.

The contrast between the form of the simulated stalagmite under high drip rates (right) compared to standard conditions is even more marked. While the total height has only increased to around 2 m, the variation in diameter is much more pronounced. Maximum growth rates have only increased from 100 to 110 μm yr^{-1}, while the diameter variation for the wet regime is between 5 and 16 cm, compared to 5–9 cm in the standard case.

We conclude that local changes in precipitation, resulting in different drip rates in a cave, produce stalagmites with different heights, and a very pronounced difference in diameter.

6.3. Variations in palaeo-CO_2 variation

Another parameter, which can change on a local scale, is the CO_2 concentration in the seepage water. An extreme case would be a landscape with small hills without vegetation cover, overlooking wide valleys covered with grasslands. Here, seepage water from the hills has a very low CO_2 concentration (it is in equilibrium with atmospheric CO_2), while water seeping through the valleys is enriched in CO_2. Different vegetation can also vary the soil-CO_2 on a smaller scale.

For our comparison, we again assume a common regional temperature variation derived from the GRIP ice core, and a standard regime with a CO_2 pressure of $p_{max} = 40.000$ ppm, a low-CO_2 regime of $p_{max} = 30.000$ ppm, and a high-CO_2 regime of $p_{max} = 50.000$ ppm. Stratigraphies for the three different regimes are shown in Fig. 14: Differences in the CO_2 regimes result in different growth rates, hence the high-CO_2 regime produces a stalagmite about 3.3 m tall (right), while in the low-CO_2 regime the height is only 0.5 m (left). The standard-regime stalagmite (middle) is again around 1.8 m tall. Differences in diameter evolution cannot be observed, as the equilibrium diameter is independent of the CO_2 concentration. We

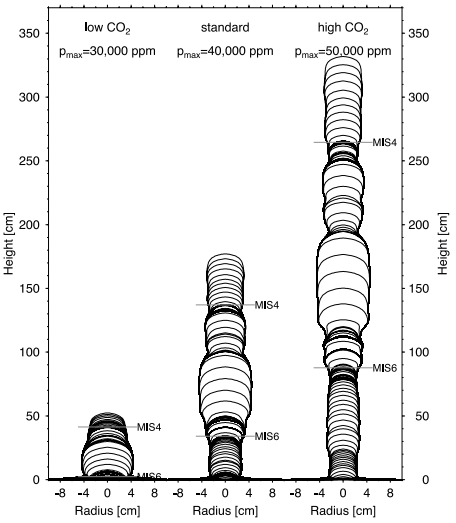

Fig. 14. Stratigraphies of stalagmites with different CO_2 concentrations. The palaeo-temperature variation is taken from the GRIP ice core (Fig. 8), and CO_2 concentrations are given in the legend. Surfaces are redrawn every 1000 yr.

derive variations in the maximum growth rates between 50 and 140 μm yr^{-1}. The diameter variations are similar for all cases, as the equilibrium diameter is independent of the CO_2 concentration, but as the CO_2 concentration also affects the calcium excess, the growth intervals become longer for the high-CO_2 regime.

7. Discussion

We have modelled stalagmite stratigraphies based on different palaeo-climate forcings. The palaeo-temperature variations are taken from observational data, while changes in palaeo-precipitation and soil cover are derived from the palaeo-temperature data using simple functions. The resulting stratigraphies show significant variations for all three palaeo-climate variables temperature, drip interval (precipitation), and CO_2 concentration (soil cover). Hence, in principle each stalagmite stratigraphy contains a unique and detailed archive about the local variability of the climate above the sample location.

From the complicated interdependence of stalagmite growth and palaeo-climate we conclude that it is difficult to infer palaeo-climate variations from a single stalagmite stratigraphy. The difficulties arise from several problems: (i) We do not know the correct relationship between temperature as master variable and both drip interval and CO_2 variation. (ii) We do not know the pathway the seepage water has taken on its way down from the surface to the cave. These uncertainties make it difficult to invert a stalagmite stratigraphy for the palaeo-climate signal, unless more observational evidence for the relationship between palaeo-temperatures and drip interval/CO_2 concentration and the percolation pathway is obtained.

Acknowledgements

The author would like to thank Wolfgang Dreybrodt for stimulating discussions on stalagmite growth. Also a big thank you to Andy Baker, Derek Ford, and Peter Smart, whose comments on the first version have greatly helped to improve the manuscript. The figures in this paper are drawn using the GMT graphics package [40,41].*[BARD]*

References

[1] C. Hill, P. Forti, Cave Minerals of the World, 2nd edn., NSS publ., 1997.
[2] S.J. Burns, D. Fleitmann, A. Matter, U. Neff, A. Mangini, Speleothem evidence from Oman for continental pluvial events during interglacial periods, Geology 29 (2001) 623–626.
[3] U. Neff, S.J. Burns, A. Mangini, M. Mudelsee, D. Fleitmann, A. Matter, Strong coherence between solar variability and the monsoon in Oman between 9 and 6 kyr ago, Nature 411 (2001) 290–293.
[4] M. Bar-Matthews, A. Ayalon, A. Kaufman, G.J. Wasserburg, The Eastern Mediterranean paleoclimate as a reflection of regional events: Soreq cave, Israel, Earth Planet. Sci. Lett. 166 (1999) 85–95.
[5] M. Bar-Matthews, A. Ayalon, A. Kaufman, Timing and hydrological conditions of Sapropel events in the Eastern Mediterranean as evident from speleothems, Soreq cave, Israel, Chem. Geol. 169 (2000) 145–156.
[6] R.S. Harmon, P. Thompson, H.P. Schwarcz, D.C. Ford, Late Pleistocene paleoclimates of North America as inferred from stable isotope studies of speleothems, Quat. Res. 9 (1978) 54–70.
[7] W. Rosendahl, A. Eisenhauer, B. Wiegand, Erste Ergebnisse von TIMS U/Th-Datierungen an Speläothemen aus einem Höhlensystem des Gottesackerplateaus (Kleinwalsertal/Allgäuer Alpen), Mitt. Verb. dt. Höhlen- und Karstforscher 44 (1998) 134–138.
[8] G. Wurth, S. Niggemann, N. Frank, A. Mangini, D.K. Richter, Jungquartäre Stalagmiten aus Höhlen des Gottesackergebietes (Allgäuer Alpen) als Archiv für Paläoumweltbedingungen, in: W. Rosendahl, S. Niggemann (Eds.), Karst und Höhle 2000/2001: Hochifen und Gottesacker, Verband dt. Höhlen- und Karstforscher, München, 2000, pp. 183–198.
[9] C. Spötl, A. Mangini, N. Frank, R. Eichstädter, S.J. Burns, Start of the last interglacial period at 135 ka: Evidence from a high alpine speleothem, Geology 30 (2002) 815–818.
[10] E. Bard, G Delaygue, F. Rostek, F. Antonioli, S. Silenzi, D.P. Schrag, Hydrological conditions over the western Mediterranean basin during the deposition of the cold Sapropel 6 (ca. 175 ka BP), Earth Planet. Sci. Lett. 202 (2002) 481–494.
[11] D.K. Richter, S. Niggemann, R. Oelze, G. Wurth, Geochemische Rhythmik und quartären Speleothemen und ihre Bedeutung für den mitteleuropäischen Raum: Ziele und erste Ergebnisse, Mitt. Verb. dt. Höhlen- und Karstforscher 43 (1997) 118–121.
[12] A. Baker, P.L. Smart, Recent flowstone growth rates:

Field measurements in comparison to theoretical predictions, Chem. Geol. 122 (1995) 121–128.
[13] A. Baker, D. Genty, W. Dreybrodt, W.L. Barnes, N.J. Mockler, J. Grapes, Testing theoretically predicted stalagmite growth rate with recent annually laminated samples: Implications for past stalagmite deposition, Geochim. Cosmochim. Acta 62 (1998) 393–404.
[14] D. Genty, A. Baker, B. Vokal, Intra- and inter-annual growth rate of modern stalagmites, Chem. Geol. 176 (2001) 191–212.
[15] W. Dreybrodt, Deposition of calcite from thin films of neutral calcareous solutions and the growth of speleothems, Chem. Geol. 29 (1980) 89–105.
[16] W. Dreybrodt, The kinetics of calcite precipitations from thin films of calcareous solutions and the growth of speleothems: revisited, Chem. Geol. 32 (1981) 237–245.
[17] D. Buhmann, W. Dreybrodt, The kinetics of calcite dissolution and precipitation in geologically relevant situations of karst areas. 1. Open system, Chem. Geol. 48 (1985) 189–211.
[18] D. Buhmann, W. Dreybrodt, The kinetics of calcite dissolution and precipitation in geologically relevant situations of karst areas. 2. Closed system, Chem. Geol. 53 (1985) 109–124.
[19] W. Dreybrodt, Chemical kinetics, speleothem growth and climate, Boreas 28 (1999) 347–356.
[20] W. Dreybrodt, H.W. Franke, Wachstumsgeschwindigkeit und Durchmesser von Kerzenstalagmiten, Die Höhle 38 (1987) 1–6.
[21] W. Dreybrodt, Processes in Karst Systems, Springer, Berlin, 1988.
[22] W. Dreybrodt, J. Laukner, L. Zaihua, U. Svensson, D. Buhmann, The kinetics of the reaction $CO_2+H_2O \rightarrow H^+ + HCO_3^-$, as one of the rate limiting steps for the dissolution of calcite in the system H_2O-CO_2-$CaCO_3$, Geochim. Cosmochim. Acta 60 (1996) 3375–3381.
[23] W. Dreybrodt, L. Eisenlohr, B. Madry, S. Ringer, Precipitation kinetics of calcite in the system $CaCO_3$-H_2O-CO_2: The conversion to CO_2 by the slow process $H^+ + HCO_3^- \rightarrow CO_2 + H_2O$ as a rate limiting step, Geochem. Cosmochem. Acta 61 (1997) 3897–3904.
[24] L.N. Plummer, T.M.L. Wigley, D.L. Parkhurst, The kinetics of calcite dissolution in CO_2-water systems at 5°C to 60°C and 0.0 to 1.0 atm CO_2, Am. J. Sci. 278 (1978) 179–216.
[25] E. Usdowski, Reactions and equilibria in the systems CO_2-H_2O and $CaCO_3$-CO_2-H_2O (0°-50°C), N. Jb. Miner. Abh. 144 (1982) 148–171.
[26] E. Busenberg, L.N. Plummer, A comparative study of the dissolution and crystal growth kinetics of calcite and aragonite, in: F.A. Mumpton (Ed.), Studies in Diagenesis, US Geol. Surv. Bull. 1578, 1986, pp. 139–168.
[27] H.W. Franke, The theory behind stalagmite shapes, Stud. Speleol. 1 (1965) 89–95.
[28] R.L. Curl, Minimum diameter stalagmites, Nat. Speleol. Soc. Bull. 35 (1973) 1–9.
[29] S.J. Johnsen, H.B. Clausen, W. Dansgaard, N.S. Fuhrer, K. Gundestrup, C.U. Hammer, P. Iversen, J. Jouzel, B. Stauffer, J.P. Steffensen, Irregular glacial interstadials recorded in a new Greenland ice core, Nature 359 (1992) 311–313.
[30] W. Dansgaard, S.J. Johnsen, H.B. Clausen, D. Dahl-Jensen, N.S. Gundestrup, C.U. Hammer, C.S. Hvidberg, J.P. Steffensen, A.E. Svelnbjörnsdottir, J. Jouzel, G. Bond, Evidence for general instability of past climate from a 250-kyr ice-core record, Nature 364 (1993) 218–220.
[31] J.R. Petit, J. Jouzel, D. Raynaud, N.I. Barkov, J.-M. Barnola, I. Basile, M. Bender, J. Chappellaz, M. Davis, G. Delaygue, M. Delmotte, V.M. Kotlyakov, M. Legrand, V.Y. Lipenkov, C. Lorius, L. Pepin, C. Ritz, E. Saltzman, M. Stievenard, Climate and atmospheric history of the past 420,000 years from the Vostok ice core, Antarctica, Nature 399 (1999) 429–436.
[32] J. Chappell, N.J. Shackleton, Oxygen isotopes and sea-level, Nature 324 (1986) 137–140.
[33] N.J. Shackleton, The 100.000 year ice-age cycle identified and found to lag temperature, carbon dioxide, and orbital eccentricity, Science 289 (2000) 1897–1902.
[34] T.C. Atkinson, K.R. Briffa, G.R. Coope, Seasonal temperatures in Britain during the past 22,000 years, reconstructed using beetle remains, Nature 325 (1987) 587–592.
[35] J. Jouzel, N.I. Barkov, J.M. Barnola, M. Bender, J. Chappellaz, C. Genthon, V.M. Kotlyakov, V. Lipenkov, C. Lorius, J.R. Petit, D. Raynaud, G. Raisbeck, C. Ritz, T. Sowers, M. Stievenard, F. Yiou, P. Yiou, Extending the Vostok ice-core record of palaeoclimate to the penultimate glacial period, Nature 364 (1993) 407–412.
[36] S. Johnsen, D. Dahl-Jensen, W. Dansgaard, N. Gundestrup, Greenland palaeotemperatures derived from GRIP bore hole temperature and ice core isotope profiles, Tellus 47 (1995) 624–629.
[37] D. Dahl-Jensen, K. Mosegaard, N. Gundestrup, G.D. Clow, S.J. Johnsen, A.W. Hansen, N. Balling, Past temperatures directly from the Greenland Ice sheet, Science 282 (1998) 268–271.
[38] N.J. Shackleton, Oxygen isotopes, ice volumes, and sea level, Quat. Sci. Rev. 6 (1987) 183–190.
[39] J.J. Drake, T.M.L. Wigley, The effect of climate on the chemistry of carbonate groundwater, Water Resour. Res. 11 (1975) 958–962.
[40] P. Wessel, W.H.F. Smith, Free software helps map and display data, EOS Trans. AGU 72 (1991) 441–446.
[41] P. Wessel, W.H.F. Smith, New, improved version of generic mapping tools released, EOS Trans. AGU 79 (1998) 579.
[42] L.N. Plummer, E. Busenberg, The solubilities of calcite, aragonite and vaterite in CO_2-H_2O solutions between 0 and 90°C, and an evaluation of the aqueous model of the system $CaCO_3$-CO_2-H_2O, Geochim. Cosmochim. Acta 46 (1982) 1011–1040.
[43] A.H. Truesdell, B.F. Jones, WATEQ, a computer program for calculating chemical equilibria of natural waters, U.S. Geol. Surv. J. Res. 2 (1974) 233–248.
[44] R.A. Robinson, R.H. Stokes, Electrolyte Solutions, Butterworths Sci. Publ., London, 1955.